Fabrication of High-Quality Opal Films with Controllable Thickness

Zhong-Ze Gu,[†] Akira Fujishima,[‡] and Osamu Sato*,[†]

Kanagawa Academy of Science and Technology, KSP Bldg. East 412, 3−2−1 Sakado, Takatsu-ku, Kawasaki-shi, Kanagawa 213-0012, Japan, and Department of Applied Chemistry, School of Engineering, The University of Tokyo, 7-3-1 Hongo Bunkyo-ku, Tokyo 113-8565, Japan

Received September 10, 2001. Revised Manuscript Received November 28, 2001

A dipping method was developed to fabricate three-dimensional colloidal crystal films. The thickness of the films fabricated by this method can be precisely controlled from one layer to several tens of layers by controlling the particle concentration and the film formation speed. Experimental results showed that the spheres form a face-centered cubic structure and that single crystals in the film can extend to centimeter dimensions.

Introduction

The self-assembly of monodispersed spheres into ordered three-dimensional structures has recently attracted great attention.[1−17] A material such as this is called a colloidal crystal or opal. Colloidal crystals have unique properties in terms of light propagation and are expected to have applications in optical devices such as photonic band gap crystals.[18−21] For most of these applications, it is critical to fabricate a high-quality colloidal crystal film with a controllable thickness. The natural sedimentation of monodispersed particles under gravity is the simplest approach for their fabrication.[22] The particles in the solvent settle under gravity and self-assemble to form a film with a cubic close-packed (ccp) structure. The major disadvantage of the sedimentation method is that it has very little control over the morphology of the top surface and the number of layers of the 3D crystalline arrays.[5] Also, it takes a long time (from weeks to months) for the submicrometer-sized particles to get completely settled. To fabricate high-quality colloidal crystal films efficiently, a number of methods that take advantage of the forces of electric fields,[10,23] the flow of gas or liquid,[6,7] and capillary force have been developed to assemble the particles to form uniform colloidal crystal films.[4] Among these, the vertical deposition method developed in Colvin's group, which utilizes capillary forces, provides a relatively simple approach to fabricating high-quality colloidal crystal films.[4]

The vertical deposition method is essentially similar to Nagayama's method,[24,25] which was mainly developed and optimized for the purpose of producing two-dimensional monolayer films. In the vertical deposition method, a substrate was first immersed vertically into a suspension containing monodispersed spheres. During the evaporation of the solvent, the surface of the solvent moves down and the film deposits onto the substrate during the decline of the solvent surface.[4] In his method, because the evaporation of the solvent was derived to control the solvent surface, the concentration of particles changes during evaporation, which may have an effect on the film thickness. To solve this problem, we fabricated colloidal crystal films by lifting the substrate out

* To whom correspondence should be addressed.
[†] Kanagawa Academy of Science and Technology.
[‡] The University of Tokyo.

(1) Blanco, A.; Chomski, E.; Grabtchak, S.; Ibisate, M.; John, S.; Leonard, S. W.; Lopez, C.; Meseguer, F.; Miguez, H.; Mondia, J. P.; Ozin, G. A.; Toader, O.; van-Driel, H. M. *Nature* **2000**, *405*, 437−440.
(2) Trau, M.; Saville, D. A.; Aksay, I. A. *Science* **1996**, *272*, 706−709.
(3) Trau, M.; Saville, D. A.; Aksay, I. A. *Langmuir* **1997**, *13*, 6375−6381.
(4) Jiang, P.; Bertone, J. F.; Hwang, K. S.; Colvin, V. L. *Chem. Mater.* **1999**, *11*, 2132−2140.
(5) Xia, Y.; Gates, B.; Yin, Y.; Lu, Y. *Adv. Mater.* **2000**, *12*, 693−713.
(6) Park, S. H.; Xia, Y. *Langmuir* **1999**, *15*, 266−273.
(7) Gu, Z.-Z.; Meng, Q.-B.; Hayami, S.; Fujishima, A.; Sato, O. *J. Appl. Phys.* **2001**, *90*, 2042−2044.
(8) Gu, Z.-Z.; Hayami, S.; Kubo, S.; Meng, Q.-B.; Einaga, Y.; Tryk, D. A.; Fujishima, A.; Sato, O. *J. Am. Chem. Soc.* **2001**, *123*, 175−176.
(9) Pan, G.; Kesavamoorthy, R.; Asher, S. A. *J. Am. Chem. Soc.* **1998**, *120*, 6525−6530.
(10) Holgado, M.; Garcia-Santamaria, F.; Blanco, A.; Ibisate, M.; Cintas, A.; Miguez, H.; Serna, C. J.; Molpeceres, C.; Requena, J.; Mifsud, A.; Meseguer, F.; Lopez, C. *Langmuir* **1999**, *15*, 4701−4704.
(11) Yoshino, K.; Kawagishi, Y.; Ozaki, M.; Kose, A. *Jpn. J. Appl. Phys.* **1999**, *38*, L786−L788.
(12) van-Blaaderen, A. *Science* **1998**, *282*, 887−888.
(13) Reynolds, A. L.; Cassagne, D.; Jouanin, C.; Arnold, J. M. *Synth. Met.* **2001**, *116*, 453−456.
(14) Johnson, N. P.; McComb, D. W.; Richel, A.; Treble, B. M.; DelaRue, R. M. *Synth. Met.* **2001**, *116*, 469−473.
(15) Romanov, S. G.; Maka, T.; Torres, C. M. S.; Muller, M.; Zentel, R. *Synth. Met.* **2001**, *116*, 475−479.
(16) Yoshino, K.; Lee, S. B.; Tatsuhara, S.; Kawagishi, Y.; Ozaki, M. Z. A. A.; Yoshino, K.; Kawagishi, Y. *Appl. Phys. Lett.* **1998**, *73*, 3506−3508.
(17) Vlasov, Y. A.; Luterova, K.; Pelant, I.; Honerlage, B.; Astratov, V. N. *Appl Phys. Lett.* **1997**, *71*, 1616−1618.
(18) Yablonovitch, E. *Phys. Rev. Lett.* **1987**, *58*, 2059−2062.
(19) John, S. *Phys. Rev. Lett.* **1987**, *58*, 2486.
(20) *Photonic Band Gaps and Localization*; Soukoulis, C. M., Ed.; Plenum Press: New York, 1993; Vol. 308.
(21) *Photonic band gap materials*; Soukoulis, C. M., Ed.; Kluwer Academic Publishers: Dordrecht, 1996; Vol. 315.
(22) Mayoral, R.; Requena, J.; Moya, J. S.; Lopez, C.; Cintas, A.; Miguez, H.; Meseguer, F.; Vazquez, L.; Holgado, M.; Blanco, A. *Adv. Mater.* **1997**, *9*, 257−260.
(23) Wen, W.; Wang, N.; Ma, H.; Lin, Z.; Tam, W. Y.; Chan, C. T.; Sheng, P. *Phys. Rev. Lett.* **1999**, *82*, 4248−4251.
(24) Denkov, N. D.; Velev, O. D.; Kralchevsky, P. A.; Ivanov, I. B.; Yoshimura, H.; Nagayama, K. *Nature* **1993**, *361*, 1303.
(25) Yamaki, M.; Higo, J.; Nagayama, K. *Langmuir* **1995**, *11*, 2975.

10.1021/cm0108435 CCC: $22.00
Published on Web 01/24/2002

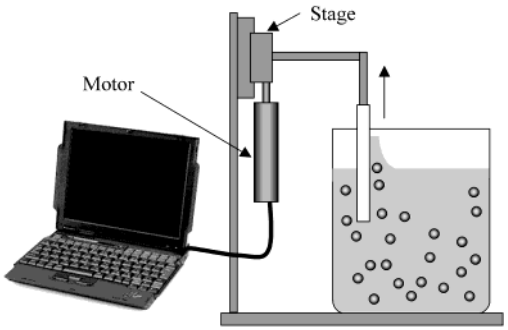

Figure 1. Outline of the film fabrication technique. The dipping apparatus is an automation stage. The movement speed of the stage is precisely controlled by a computer.

of the suspension at a constant speed instead of relying on the evaporation of the solvent. It will be shown that face-centered cubic (fcc) colloidal crystal films with uniform color can be fabricated by this method. The thickness of the film can be controlled from just a single layer to several tens of layers by changing the particle concentration or the lifting speed. Because the concentration of the particles in the suspension is almost constant, uniform films extend to several centimeters.

Experimental Section

Materials and Equipment. Monodispersed polystyrene and fluorescence spheres of varying diameters were bought from the Duke Scientific Corporation (U.S.A.) or the Interfacial Dynamics Corp. (U.S.A.). The fluorescence particles are a product obtained from Polysciences, Inc., U.S.A. Reagent quality sulfuric acid (95%) and hydrogen peroxide (30%) were bought from Wako Chemical (Japan). Slide glasses and cover glasses are the products from Iwaki Glass, Inc., (Japan). Deionized water was used for the experiments.

The dipping machine is an automation stage controlled by a computer (Figure 1). The dipping speed can be varied over a range of 0.1−70 μm/s. UV−vis spectra were recorded on a Shimadzu model UV-3100PC spectrophotometer. Scanning electron microscope (SEM) observations were performed using a JEOL model JSM-5400 SEM, and microscopic observations were performed by using an Olympus IX70 inverse type microscope equipped with a CCD camera. A Filmetric F20 thin-film measurement system was used for the film thickness measurements.

Substrate and Treatment. The slide glasses and cover glasses used for the experiment were first treated with a solution containing 30% hydrogen peroxide and 70% sulfuric acid overnight. Then, the glass substrates were rinsed with deionized water and dried under a flow of dried air or nitrogen gas. The glass substrates after the treatment are hydrophilic. The contact angles of water on the substrates were measured as 0°.

Fabrication of Films. Figure 1 depicts the scheme for the fabrication of the colloidal crystal film. Experimental procedures are as follows: First, a suspension of the particles was diluted to a definite concentration using deionized water. Then, a hydrophilic glass substrate was immersed vertically into the dispersion and lifted up with a constant speed, which was precisely controlled by a motor. The temperature for the experiment was set at 23 °C.

Characterization of Film. Film thickness was determined by using SEM or a thin-film measurement system. The samples for SEM observation were scraped by using a sharp razor blade and then sputtered with thin gold films. The SEM was also used for the observation of the particle arrangement in the colloidal crystal films. Since the SEM can obtain information only about the surface of the colloidal crystal films, a microscope was used to observe the three-dimensional crystal structure. The colloidal crystal films for the microscopic observation were fabricated on cover glass substrates by using fluorescence particles. Matching liquid was infiltrated into the film to decrease the mismatch of the refractive indices between the spheres and air. The images were recorded by using a CCD camera and analyzed by using Image Pro, a commercial image-processing software.

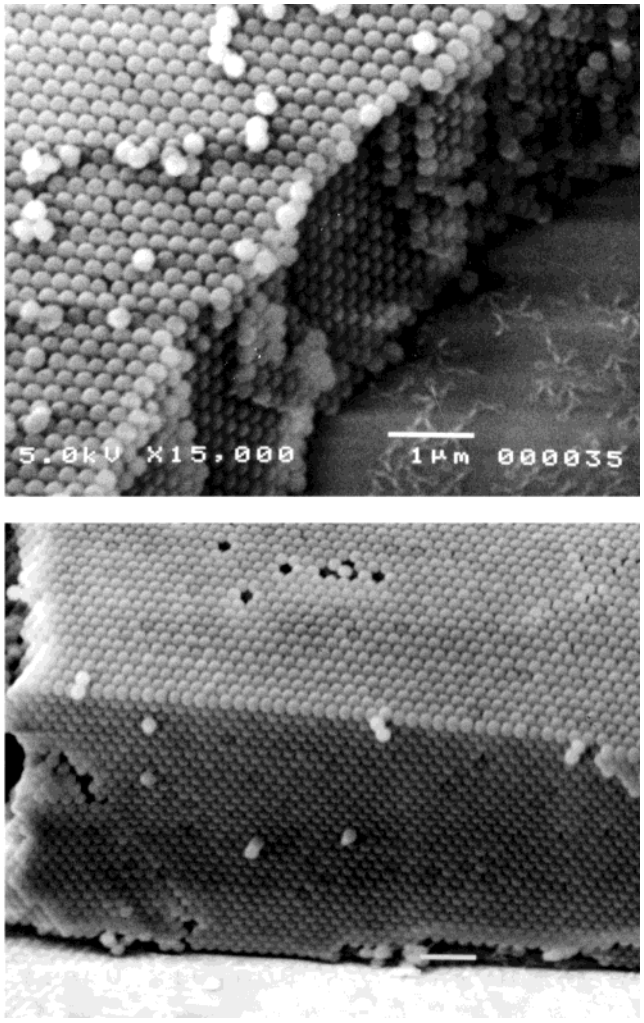

Figure 2. Cross-sectional images of colloidal crystals composed of spheres with a diameter of 246 nm: (a) film fabricated at a speed of 0.2 μm/s using a 1.5% (v/v$_0$) suspension; thickness is 15 layers and (b) film fabricated at a speed of 0.1 μm/s using a 3% (v/v$_0$) suspension; thickness is 31 layers.

Result and Discussion

Control of Film Thickness. The film thickness of the colloidal crystal films can be controlled by changing either the particle concentration or the lifting speed. In Figure 2, cross-sectional images of the colloidal crystal films fabricated under different conditions are exhibited. Figure 2a is the film fabricated with a lifting speed of 0.2 μm/s using a suspension with 1.5% (v/v$_0$) of particles. Under these conditions, a film with a thickness of 15 layers was derived. Figure 2b shows a film fabricated at a speed of 0.1 μm/s using a 3% (v/v$_0$) suspension. The thickness of the film is 31 layers. Film thickness is apparently a function of both the concentration and the lifting speed. Either of these two factors may be used to control the number of layers.

The detailed experimental results showing how the concentration and lifting speed affect the film thickness

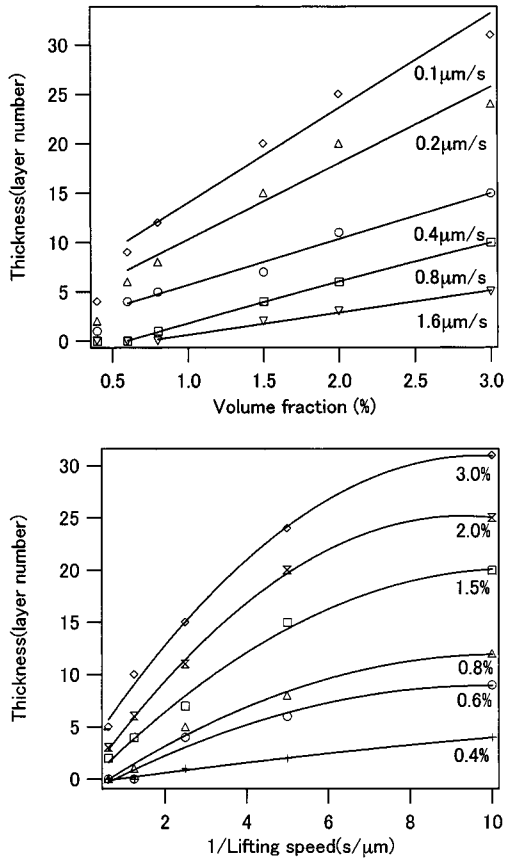

Figure 3. Dependence of the film thickness, composed of spheres with a size of 246 nm, on the concentration and lifting speed: (a) The relationship between the film thickness and volume fraction of spheres. The relationship is tested at six different lifting speeds, which are indicated as different marks. The lines are the best-fit results using a linear function. (b) The relationship between thickness and the inverse of the lifting speed. The different marks represent films fabricated using suspensions with different concentrations. The lines in the graph are the best-fit results using a second-order polynomial function.

are shown in Figure 3. Figure 3a is the relationship between the film thickness and particle concentration. The volume fractions used for fabrication were varied from 0.4 to 3% (v/v_0). Each different suspension was used to fabricate films at five different lifting speeds, varying from 0.1 to 1.6 μm/s. From this graph, it can be observed that in the concentration region between 0.6 and 3% (v/v_0), the film thickness increases linearly with the volume fraction. The theoretical relationship between the thickness and the concentration is[26]

$$k = \frac{\beta L j_e \varphi}{0.605 d v (1 - \varphi)} \quad (1)$$

where k is the layer number, v is the growth rate of the film determined by lifting speed, φ is the particle volume fraction, j_e is the solvent evaporation rate, d is the diameter of colloidal spheres, L is the meniscus height, and β is the ratio between the velocity of a particle in solution and the fluid velocity. A linear relationship between the film thickness and concentration is expected from eq 1, which agrees with the experimental results. From these results, it was also found that the slopes of the lines are increased by decreasing the lifting speed, which means that the film thickness is more sensitive to the concentration change at low lifting speeds. It should be noted here that for those films fabricated from a suspension whose concentration is lower than 0.4% (v/v_0), the film thicknesses are thinner than those expected from the extrapolation of the lines derived from the results with concentrations larger than 0.6% (v/v_0).

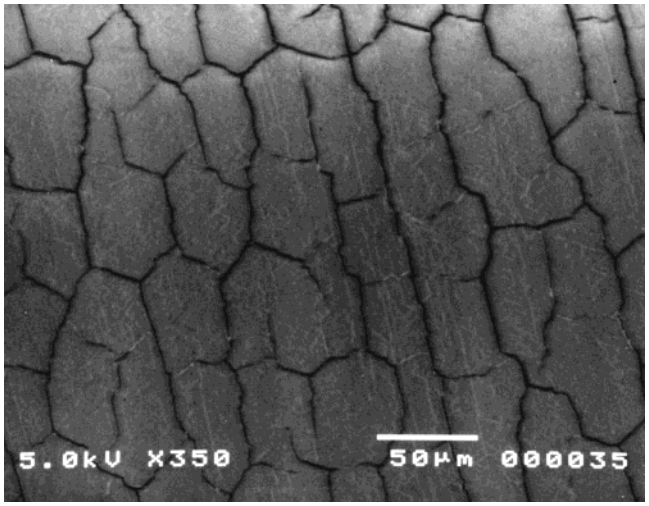

Figure 4. Low-magnification SEM image of a film composed of spheres with a diameter of 288 nm.

The relationship between the film thickness and lifting speed is shown in Figure 3b. Six suspensions with particle concentrations from 0.6 to 3% (v/v_0) were used to test the influence of lifting speed. To compare the experimental results with the theoretical prediction obtained from eq 1, the graph is drawn as the number of layers vs the inverse of the lifting speed. From eq 1, a linear relationship between the number of layers and the inverse of the lifting speed is expected if all of the other parameters are kept constant. Such linear relationships were not found in the experimental results. Figure 3b shows that the films fabricated at low lifting speeds are always thinner than the linear expectation based on the data derived from high-speed fabrication. Such phenomena could be due to changes in solvent evaporation speed, because in the case where films are fabricated at high lifting speed, the spheres crystallize at a position farther from the solvent surface than for those fabricated at low speed. Therefore, the evaporation speed of the solvent is slowed at low lifting speeds. From eq 1, such a change can decrease the film thickness. It was found that the relationship between the film thickness and the inverse of the lifting speed can be best fitted by a second-order polynomial function. The fitting results are exhibited as lines in Figure 3b.

Observation of Crystal Structure. The morphologies of the colloidal crystal films were first observed by SEM. One typical low-magnification image, which gave information about the surface of the film over a wide area, is shown in Figure 4. The low-magnification images show that the flat surfaces of the film can extend to a very a large region on which cracks exist. The distances between the cracks vary from 10 to 100 μm. This morphology is similar to that observed in the films fabricated by other methods.[4] The appearance of the

(26) Dimitrov, A. S.; Nagayama, K. *Langmuir* **1997**, *12*, 11303.

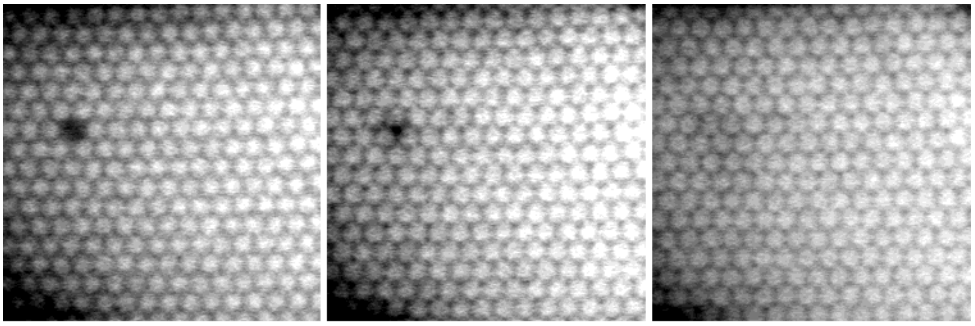

Figure 5. Fluorescence microscopic images of a film composed of spheres with a diameter of 737 nm: (a), (b), and (c) are three consecutive layers, starting from the glass substrate. The images are the original images without any image processing.

cracks was ascribed to the shrinkage of the spheres during the drying process. The arrangements of the spheres in the films were initially observed from a high-magnification SEM image. A top-view image of the film is shown in Figure 8. A hexagonal arrangement of the spheres was observed almost everywhere, indicating that the spheres were arranged well in the planar layer. The high degree of regularity is also reflected in the fast Fourier transform (FFT) images (Figure 8), which exhibit clear patterns for all of the SEM images. Information about the state of the planar arrays can be derived from the cross-sectional images (Figure 2). Apparently, the planar arrays pile up regularly from the substrate to the surface of the film. The results from the SEM observations indicate that the spheres form a ccp structure in the films.

In the colloidal crystal films with the ccp structure, the planar arrays of spheres were originally thought to be arranged as ABCABC... (face-centered cubic (fcc) structure), ABAB... (hexagonal close-packed (hcp) structure), or randomly packed. Theoretical calculations show that the energy differences between the three types of structure are small.[27] As SEM images can give information only about the top surface or the vertical cross section, distinguishing the crystalline forms between the structures is impossible. A method for the observation of the three-dimensional arrangement of spheres is necessary. Here, we used a fluorescence microscopic observation technique to determine the crystal structure.

Microscopic observation is a technique used for the observation of colloidal crystals suspended in solution.[28−32] Because the spheres in solution are well separated and the mismatch between the refractive indices of the spheres and solution is small, a three-dimensional arrangement of spheres can be easily observed optically. The situation is somewhat different for the dried colloidal crystals. For dried colloidal crystal films composed of fluorescence spheres with a size of 737 nm, only the image of the outmost layer is observable. The images of the inner layers are blurred due to the strong light scattering between the spheres and air. To reduce the scattering, a matching liquid with a refractive index close to that of the spheres was infiltrated into the void of the colloidal crystals. The film becomes completely transparent after the infiltration. After this treatment, the samples were used for the microscopic observation.

Figure 5 shows the microscopic images of the sample treated by this method. Three layers starting from the substrate are shown. Apparently, the quality of the image of the inner layer remains constant. Such an image quality is maintained for over 10 layers. These images were recorded by a CCD camera and used for the analysis of the stereostructure. The identification and measurement of the position of spheres in the images was performed by using the image-processing software, Image Pro. The derived coordinates were used for reconstruction and analyses.

Figure 6a shows the projections of the three layers along the direction vertical to the substrate. Apparently, there is no overlap between the positions of the spheres in the different layers, indicating that the layers stack in the ABC form. The spheres in the fourth layer return to the same position as those which were occupied by the spheres in the first layer, and the stacking pattern was repeated again (Figure 6b). Figure 7 shows the three-dimensional stereoscopic structure of the colloidal crystal reconstructed from the microscopic images. The blue spheres in the pictures are those around a point defect in the colloidal crystal. Apparently, such a defect does not affect the structure in the next layer. From this observation, it can be concluded that the spheres form the fcc structure in the films fabricated by the dipping method.

To determine the long-range ordering of the crystalline structure, SEM images of the colloidal crystal films at different positions were recorded. The size of the sample for the observation is about 1.5 cm × 2.6 cm. The observation method is as follows: first, we observed the arrangement of the spheres at one position of the film and then used the XY stage to transfer the sample to another definite position and obtained the image of the spheres there. Images taken at two positions separated by 1 cm are shown in Figure 8. The two SEM images were placed closely one above the other for the purpose of comparing the periodicity and orientation of the lattices in the two images. Apparently, they agree very well, although the images were recorded at positions separated by 1 cm. Such a good conformity is also

(27) Woodcock, L. V. *Nature* **1997**, *385*, 141−143.
(28) Kose, A.; Ozaki, M.; takano, K.; Kobayashi, Y.; Hachisu, S. *J. Colloid Interface Sci.* **1973**, *44*, 330−338.
(29) Yoshida, H.; Yamanaka, J.; Koga, T.; Ise, N.; Hashimoto, T. *Langmuir* **1998**, *14*, 569−574.
(30) Blaaderen, A. V.; Ruel, R.; Wiltzius, P. *Nature* **1997**, *385*, 321−324.
(31) He, Y. M.; Ackerson, B. J. *Physica A* **1997**, *235*, 194−203.
(32) Gu, Z.-Z.; Fujishima, A.; Sato, O. *J. Am. Chem. Soc.* **2000**, *122*, 12387−12388.

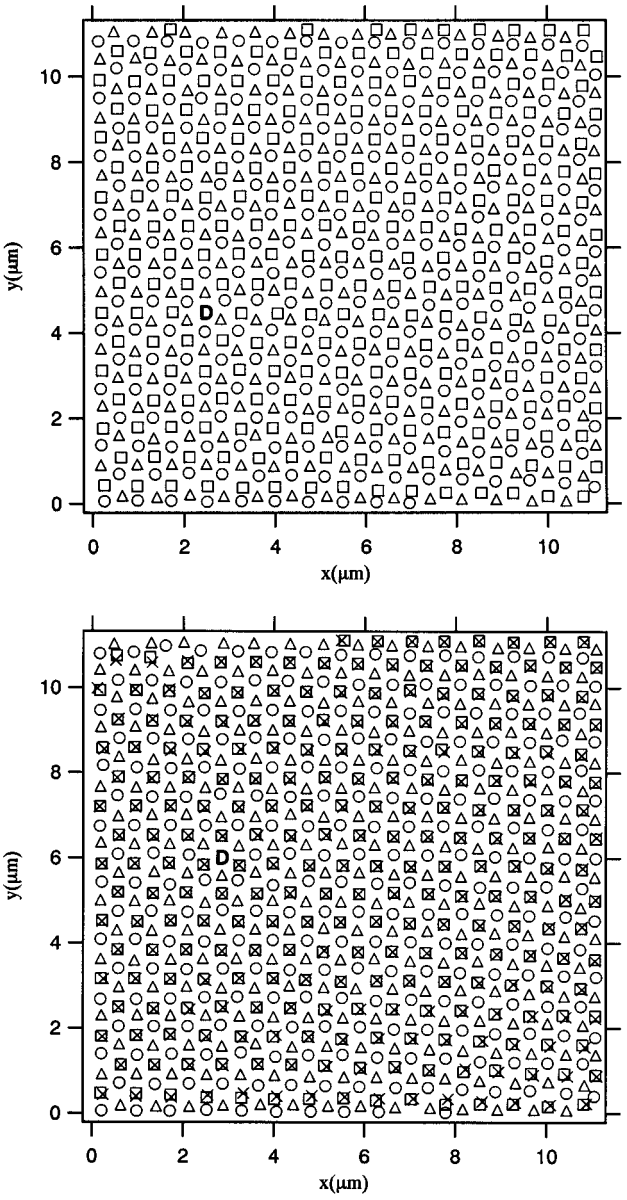

Figure 6. Projection of spheres in the different layers on a plane parallel to the substrate: (a) projection of the spheres exhibited in Figure 6; □, ○, and △ represent the spheres in the first, second, and third layers, respectively and (b) projection of the spheres in the fourth to seventh layers, which are represented as □, ○, △, and × correspondingly. Character D in the graphs represents the positions of point defects.

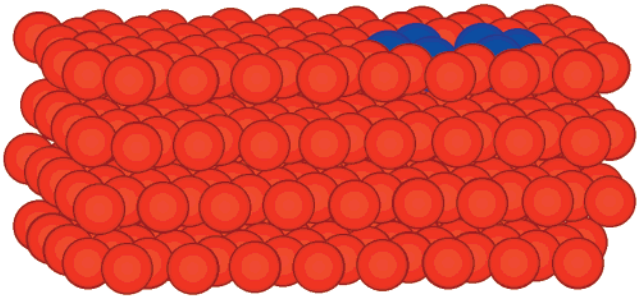

Figure 7. Stereoscopic pictures of a colloidal crystal reconstructed using the images in Figure 6.

supported by their FFT images. The above results indicate that the long-range ordering of the spheres can reach centimeter dimensions. The long-range ordering has no correlation with the cracks in the films, implying that the cracks probably appear after the formation of the crystal.

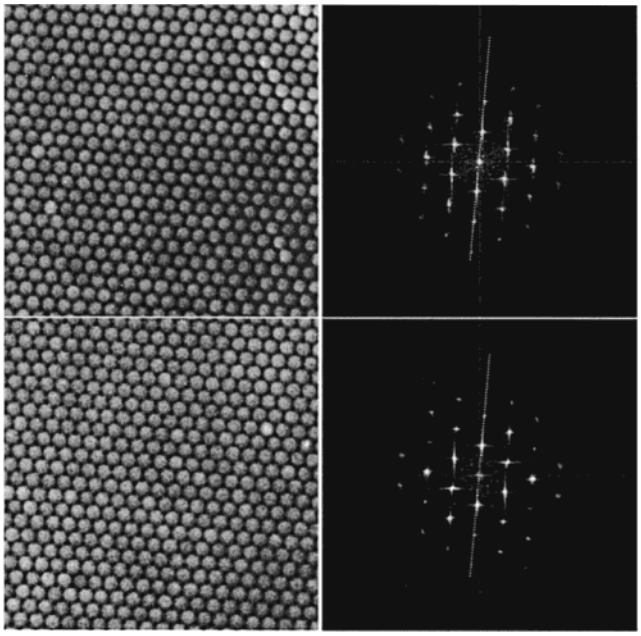

Figure 8. Sphere arrangements in a film composed of spheres with a diameter of 288 nm. The left-hand images are the SEM images taken at two positions separated by 1 cm. The right-hand images are the corresponding FFT images. The dashed lines in the FFT images represent the reference direction. The alignment of the dots in both of the FFT images agrees with the reference direction very well.

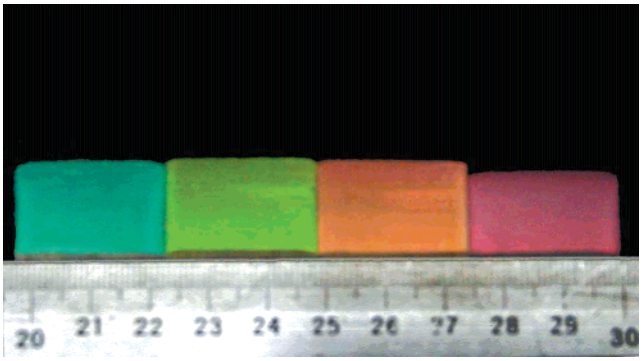

Figure 9. Photograph of colloidal crystal films composed of polystyrene spheres of different sizes. The diameters of the spheres are 211, 233, 246, and 263 nm from left to right, respectively.

Optical Properties. The high optical quality of the film can be judged by the naked eye. A uniformly brilliant color that extends to centimeter dimensions can be observed for all of the films whose stop bands are in the visible range. Figure 9 shows photographs of four colloidal crystal films composed of different sizes of spheres. The colors of the films change from blue to red with increasing sphere size. Detailed information on the optical properties of the opal films was derived by the measurement of UV−vis spectra. Figure 10 shows the transmission spectra of the colloidal crystal film composed of spheres with a size of 246 nm. The relative stop bandwidth of $\Delta\lambda/\lambda_0$, where $\Delta\lambda$ is the width at half-maximum of the peak and the λ_0 is the center wavelength of the peak, is 7%. This value agrees approximately with the theoretical calculation result for an fcc

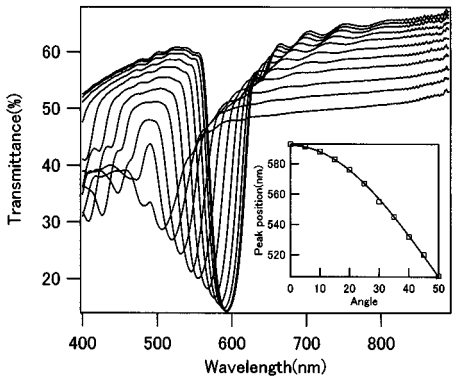

Figure 10. Transmission spectra of a film composed of spheres with a diameter of 246 nm. The angle between the normal line of the film surface and the detecting light changes from 0 to 50°, and the spectra were recorded every 5°. Inset shows the relationship between the peak position and detecting angle (□). The experimental results were fitted by the Bragg formula (eq 2).

crystal.[33] The peak positions in the spectra depend on the angle between the normal vector of the substrate and the detecting light and they shift to shorter wavelength with increasing detection angle. The spectra measured at different angles are given in Figure 10. The relationship between the peak position and the detecting angles is summarized in the inset and fitted by the Bragg formula

$$\lambda_{max} = (8/3)^{1/2} D(n_{sphere}^2 V_{sphere} + n_{void}^2 V_{void} - \sin^2 \phi)^{1/2} \quad (2)$$

where D is the diameter of the sphere, which in this case is 246 nm. n_{sphere} and n_{void} are the refractive indices of the spheres and voids, respectively. The values are 1.6 for polystyrene spheres and 1 for air voids. V_{sphere} and V_{void} are the volume fractions of spheres and voids in the crystal and they are 0.74 and 0.26, respectively, in the fcc structure. Apparently, the experimental results agree well with the calculation. This result supported the conclusion that the films are composed of a well-crystallized fcc structure as previously derived from SEM and microscopic observations.

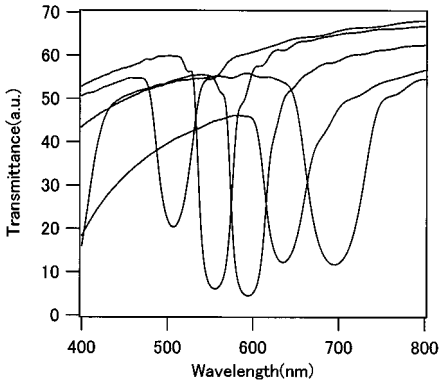

Figure 11. Transmission spectra of a film composed of different spheres. The spectra with transmission peak shifts from short wavelength to long wavelength are the films composed of spheres with diameters of 211, 233, 246, 263, and 288 nm.

Sharp attenuation peaks can be observed for all of the films fabricated by this method. The transmission spectra of five films composed of different sizes of spheres are shown in Figure 11. The position of the peak shifts to longer wavelength with increasing sphere size. The relationship between the peak position and sphere size can also be well fitted by the Bragg formula (eq 2). This result indicates that well-crystallized films can be derived for all of these spheres.

Conclusion

We demonstrated a dipping method for the fabrication of high-quality, uniform opal films. The film thickness is easily controlled by either the particle concentration or the lifting speed. The spheres in the films fabricated by this method crystallize in the form of the fcc structure. The single-crystal size can extend to an order of centimeters.

Acknowledgment. This work was supported in part by the Japan Society for the Promotion of Science and the Kanagawa Prefecture Joint-Research Project for Regional Intensive, Japan Science and Technology Corporation.

CM0108435

(33) Tarhan, I. I.; Watson, G. H. *Phys. Rev. B* **1996**, *54*, 7593−7597.